

7 **Pt Monolayer Shell on Nitrided Alloy Core — A Path to Highly**  
8 **Stable Oxygen Reduction Catalyst**9 **Jue Hu <sup>a,b</sup>, Kurian A. Kuttiyiel <sup>a</sup>, Kotaro Sasaki <sup>a\*</sup>, Dong Su <sup>a</sup>, Tae-Hyun Yang <sup>c</sup>, Gu-Gon Park <sup>c\*</sup>,**  
10 **Chengxu Zhang <sup>b</sup>, Guangyu Chen <sup>a</sup>, Radoslav R. Adzic <sup>a\*</sup>**11 <sup>a</sup> Chemistry Department, Brookhaven National Laboratory, Upton, NY 11973, USA.12 <sup>b</sup> Hefei Institutes of Physical Science, Chinese Academy of Sciences, P. O. Box 1126, 230031, P. R.  
13 China.14 <sup>c</sup> Fuel Cell Research Center, Korea Institute of Energy Research, Daejeon, 305-343, Korea.

15 \* Author to whom correspondence should be addressed; E-Mail: adzic@bnl.gov;

16 Tel.: +1-631-344-4522; Fax: +1-631-344-5815. E-Mail: ksasaki @bnl.gov;

17 Tel.: +1-631-344-3446. E-Mail: gugon@kier.re.kr; Tel.: +82-42-860-3782.

18 Academic Editor:

19 *Received: / Accepted: / Published:*  
20

---

21 **Abstract:** The inadequate activity and stability of Pt as a cathode catalyst under the severe  
22 operation conditions are the critical problems facing the application of the proton exchange  
23 membrane fuel cell (PEMFC). Here we report on a novel route to synthesize highly active  
24 and stable oxygen reduction catalysts by depositing Pt monolayer on a nitrided alloy core.  
25 The prepared Pt<sub>ML</sub>PdNiN/C catalyst retains 89% of the initial electrochemical surface area  
26 after 50000 cycles between potentials 0.6 and 1.0 V. By correlating electron energy-loss  
27 spectroscopy and X-ray absorption spectroscopy analyses with electrochemical  
28 measurements, we found that the significant improvement of stability of the Pt<sub>ML</sub>PdNiN/C  
29 catalyst is caused by nitrogen doping while reducing the total precious metal loading.30 **Key words:** Nickel Nitride; ORR; Electrocatalyst; Core-Shell; Stability, Pt monolayer.  
31

## 33 1. Introduction

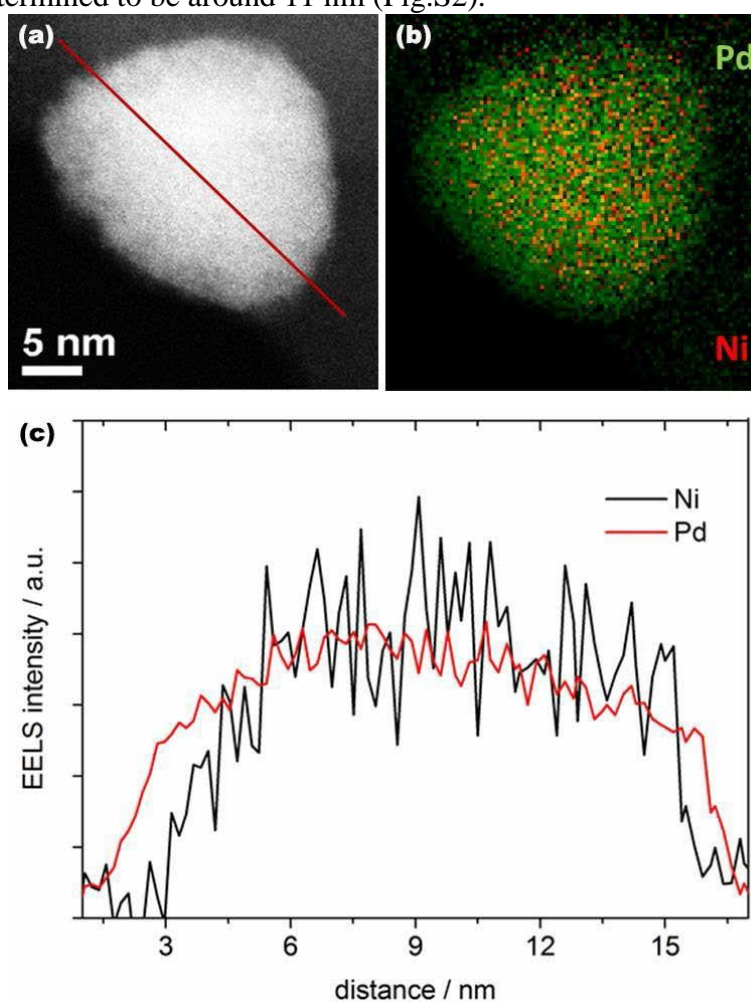
34 Proton exchange membrane fuel cell (PEMFC) is expected to be an alternative power-generation for  
35 vehicles, stationary and portable power applications because of its high energy density, low operation  
36 temperature, low air pollution and the use of renewable fuels, such as hydrogen and some alcohol [1,2].  
37 Although the PEMFC power source technique has been really influent in the last decade, the slow  
38 kinetics of the oxygen reduction reaction (ORR) is still one of the main obstacles hampering the large  
39 scale applications of PEMFC [3]. Platinum (Pt) as the most effective catalyst for ORR has been the  
40 general choice. However, the high Pt loading at the cathode as well as the inadequate activity and  
41 stability of Pt under the severe operation condition are still the unresolved problems facing the PEMFC  
42 [4,5]. To overcome these problems, it is essential to decrease the Pt amount in electrocatalysts, and at the  
43 same time, improve the performance of the Pt-based cathode catalyst both in terms of activity and  
44 stability. To this end, one of the strategies is to develop the metal@Pt core-shell structure catalysts in  
45 which a non-Pt core is employed and covered by atomically thin layers of Pt. This core-shell structure  
46 allows efficient use of Pt, and thereby can reduce the demands on Pt while enhancing the catalyst  
47 performance [6-9].

48 Significant progress has been made through the combination of experimental and theoretical  
49 studies[10,11]. We developed a new class of catalysts consisting of a Pt monolayer on different metals  
50 and alloy supporting cores, including Pd, Ru, Ir, Rh, Au, PdAu, IrNi, IrRe, and AuNiFe [12-18]. The  
51 ORR activity of Pt monolayer on different metal surfaces show a volcano-type dependence on the  
52 d-band center of Pt [18]. The strain-induced d-band center shifts and electronic ligand effects between  
53 the substrate and the overlayer are the two main factors determining the activity of these core-shell  
54 catalysts [6]. Nevertheless, the improvement of the electrocatalytic activity and stability of Pt-based  
55 cathode catalysts simultaneously is still a challenge. Great efforts have been made to modifying the  
56 Pt surface with other elements such as Au [19]. The oxidation of Pt on this Au modified Pt surfaces  
57 requires much higher potentials than that on unmodified Pt surface, resulting in the enhancement of the  
58 catalyst stability [19]. Another strategy is to modify the metal core. Gong et al. synthesized highly stable  
59  $Pt_{ML}AuNi_{0.5}Fe$  catalysts and found that the Au shell in the core precluded the exposure of NiFe to the  
60 electrolyte leading to the high electrochemical stability [20]. Kuttiyiel et al. also developed a highly  
61 stable ORR catalyst by Au-stabilized PdNi [21]. More recently, we have reported a new approach to  
62 develop Pt-M (Ni, Co, and Fe) core-shell catalysts with high stability and activity by nitriding core  
63 metals [22,23]. The synchrotron XRD analysis proved the generation of the highly stable  $Fe_4N$ ,  $Co_4N$   
64 and  $Ni_4N$  nitride cores. Since the Pt monolayer on Pd core catalyst is on the top of the volcano plot as  
65 mentioned above, and also the price of Pd is considerably lower than that of Pt [24], we selected Pt  
66 monolayer on nitride stabilized PdNi core ( $Pt_{ML}PdNiN$ ) for studying in detail it's synthesis and structure  
67 with the possibility to simultaneously improve its stability and activity, while reducing the PGM metal  
68 content.

## 69 2. Results and Discussion

70 PdNi alloy nanoparticles were first synthesized by chemical reduction (see experimental section),  
71 followed by thermal annealing in  $N_2$  at 250 °C for 1 h, and subsequent annealing at 510 °C for 2 h in  $NH_3$   
72 as the nitrogen precursor. As illustrated in Fig. 1, the PdNiN nanoparticles have a core-shell structure

73 with Ni in the core and Pd on the surface. Fig. 1a shows a high angle annular dark field scanning  
74 transmission electron microscope (HAADF-STEM) image of a representative single PdNiN  
75 nanoparticle. Elementary characterization of the PdNiN nanoparticle was performed by the electron  
76 energy-loss spectroscopy (EELS) mapping for Pd (M-edge, 2122 eV) and Ni (L-edge, 855 eV) from the  
77 nanoparticle shown in Fig. 1a. As shown in Fig. 1b, overlapping the mapping of Pd and Ni EELS signal  
78 validates an obvious Ni-core and Pd-shell structure. However, the outside of the particle is decorated by  
79 a trace amount of Ni/Ni oxides. The Ni/Ni oxides would not affect the electrocatalytic activity of these  
80 particles because they quickly dissolve in acid conditions during the Pt monolayer deposition. Fig. 1c  
81 and Fig.S1 (Supplementary Information) shows a line profile analysis by STEM-EELS illustrating the  
82 distribution of the Pd and Ni components in a single representative nanoparticle. It is evident that the Pd  
83 atoms are distributed uniformly over the Ni; the Pd shell thickness is determined to be around 0.6-1.5 nm  
84 by examining a number of particles. From the TEM images, the average particle size of the PdNiN  
85 nanoparticles was determined to be around 11 nm (Fig.S2).



86

87 **Fig.1.** (a) HAADF-STEM image of PdNiN core-shell nanoparticle. (b) Two dimensional  
88 EELS mapping of Ni L signal (red) and Pd M signal (green) from a single nanoparticle. (c)  
89 EELS line scan profile for Pd M-edge and Ni L-edge along the scanned line indicated in (a).

90 To verify the formation of NiN<sub>x</sub> core in PdNiN nanoparticles we carried out X-ray absorption  
91 spectroscopy (XAS) measurements and compared the obtained spectra with those of reference metal  
92 foils, as shown in Fig.2. X-ray absorption near-edge structure (XANES) of Ni K edge from PdNiN

nanoparticles shows that the electronic state of Ni has been changed due to the presence of N forming NiN<sub>x</sub> species. The Fourier transform (FT) magnitudes of the extended x-ray absorption fine structure (EXAFS) data for Ni-K edge (Fig. 2c) for PdNiN presents a decrease in Ni bonding distance due to the formation of Ni nitrides. Also previous studies have shown that EXAFS for NiO or Ni(OH)<sub>2</sub> species demonstrate a peak at 1.6 Å corresponding to the Ni-O bond, accompanied by small peak at around 2.4 Å corresponding to the Ni-Ni bond [25]. The absence of these peaks along with the changes in the bonding distance compared to Ni metal verifies the presences of N<sub>x</sub> species in the PdNiN. The alloying effect of PdNiN<sub>x</sub> has changed the electronic states of Pd as well, and these distinctions are clearly observed in the XANES and EXAFS regions when compared to those from a Pd foil (Fig. 2b and d). The appearance of a peak around 2.0 Å in FT EXAFS of Pd K edge for PdNiN is likely caused by Pd-Ni bond. Although the exact species of NiN<sub>x</sub> could not be determined, the XAS results along with the STEM-EELS analysis indicate that Ni in the core-shell structured PdNiN nanoparticles is nitrated. Our previous studies on nitrated Pt-M (M= Ni, Fe or Co) core-shell nanoparticles have indicated the presences of M<sub>4</sub>N species [22,23]. As the synthesis parameters are similar to the previous study we presume the presence of Ni<sub>4</sub>N species in our PdNiN core-shell nanoparticles.

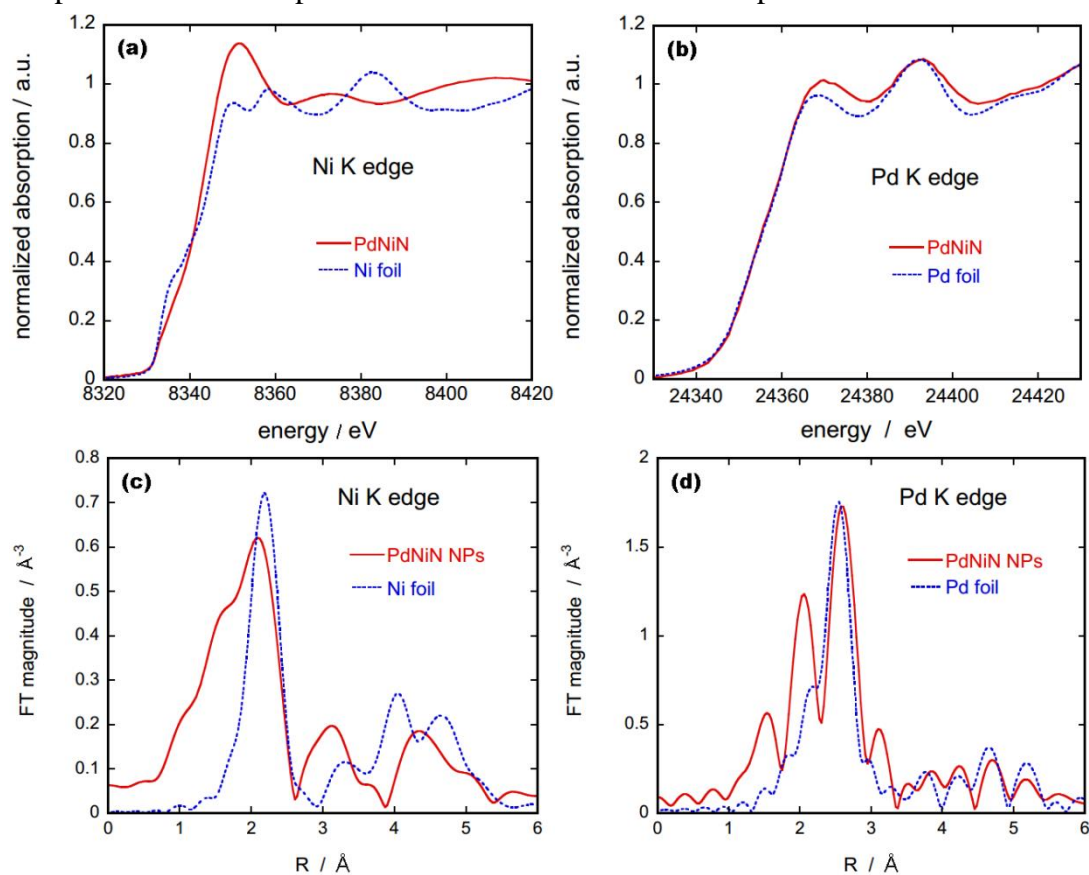


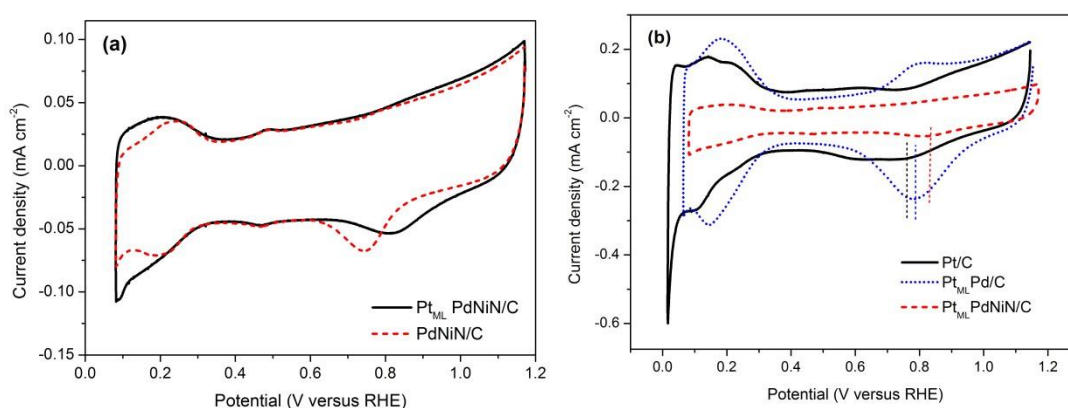
**Fig. 2.** (a, b) Normalized XANES spectra for Ni and Pd K edges respectively along with Ni and Pd reference foil. (c, d) FT EXAFS spectra for Ni and Pd K edges respectively along with their reference foils.

The cyclic voltammetry (CV) curves obtained on the PdNiN/C and Pt<sub>ML</sub>PdNiN/C catalysts in Ar-saturated 0.1M HClO<sub>4</sub> solution are shown in Fig. 3a. It is observed that the curves in the hydrogen adsorption/desorption region of the Pt<sub>ML</sub>PdNiN/C resembled to those of a typical Pt/C surface although the peaks from (110) and (100) planes are suppressed due to the interaction of the substrate materials.

117 Moreover, after a Pt<sub>ML</sub> depositing on the PdNiN/C surface, the oxide adsorption/desorption potentials  
 118 shift more positively. The surface area of *i*-*E* plot associated with the hydrogen desorption can be used to  
 119 estimate the electrochemical surface area (ECSA) of Pt catalysts. The ECSA of catalyst can be  
 120 calculated according to Eq. (1) [26]:

$$121 \quad S_{\text{ECSA}} = \frac{Q_{\text{H}}}{L_{\text{Pt}} \times 0.21} \quad (1)$$

122 in which  $L_{\text{Pt}}$  represents the Pt loading ( $1.13 \mu\text{g cm}^{-2}$  derived from the Cu under-potential deposition  
 123 charge),  $Q_{\text{H}}$  ( $\text{mC cm}^{-2}$ ) is the charge-exchanged during the electro-desorption of hydrogen on Pt  
 124 surface and  $0.21$  ( $\text{mC cm}^{-2}$ ) is the charge required to oxidize a monolayer of hydrogen on a smooth Pt  
 125 [27]. The ECSA value of the catalyst is  $90 \text{ m}^2 \text{ g}^{-1}_{\text{Pt}}$ . Comparison of CVs from the commercial Pt/C  
 126 (E-TEK, 10 wt%), Pt<sub>ML</sub> deposited commercial Pd/C (E-TEK, 10 wt%, 3.5nm Pd particle size) and  
 127 Pt<sub>ML</sub>PdNiN/C catalysts (Fig. 3b) showed that the oxide adsorption/desorption wave of Pt<sub>ML</sub>PdNiN/C  
 128 occurred 37 mV and 60 mV positive compared to the Pt<sub>ML</sub>Pd/C and commercial Pt/C catalyst,  
 129 respectively. The elevation of Pt oxidation potential on the Pt<sub>ML</sub>PdNiN/C catalyst indicates stabilization  
 130 of the Pt<sub>ML</sub> on the PdNiN/C substrate [19].



131

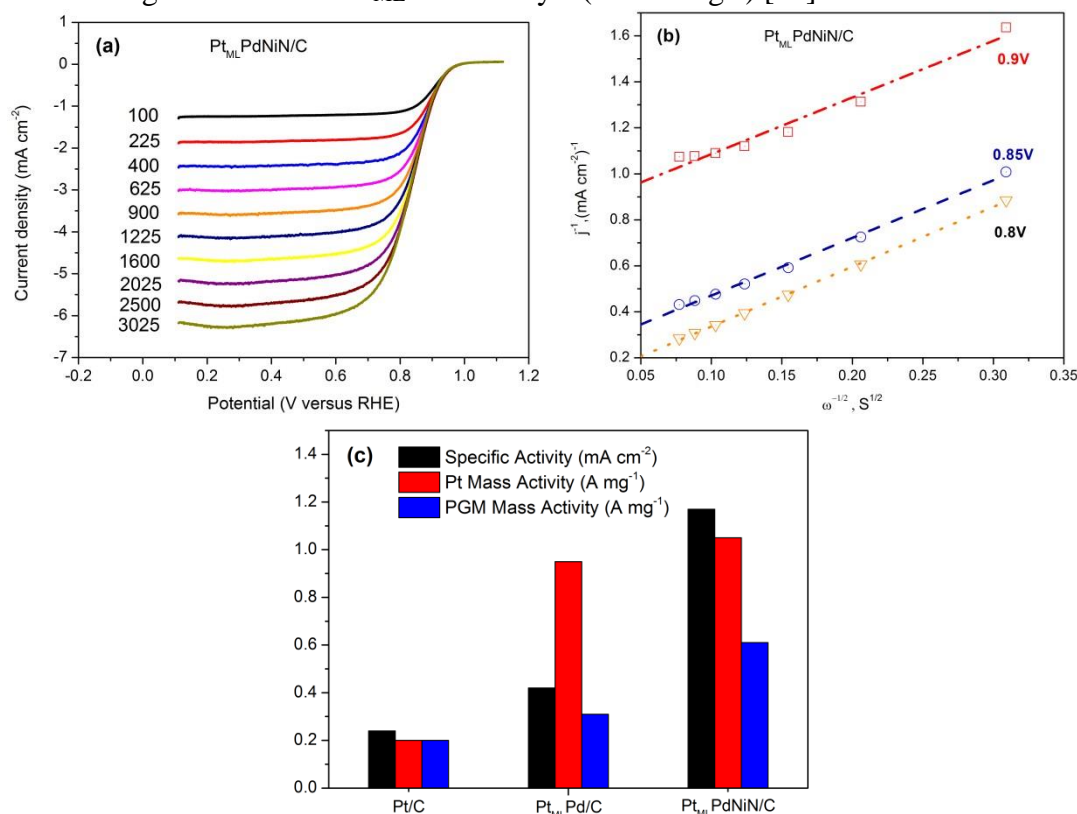
132 **Fig. 3.** Cyclic voltammograms for (a) obtained PdNiN/C and Pt<sub>ML</sub>PdNiN/C, and (b)  
 133 commercial Pt/C, Pt<sub>ML</sub>Pd/C and Pt<sub>ML</sub>PdNiN/C nanoparticles in 0.1 M HClO<sub>4</sub> solution at a  
 134 scan rate of 20 mV s<sup>-1</sup>.

135 Fig. 4a shows rotating disk electrode (RDE) measurements of the ORR on the Pt<sub>ML</sub>PdNiN/C catalyst  
 136 in O<sub>2</sub> saturated 0.1 M HClO<sub>4</sub> solution at a sweep rate of 10 mV s<sup>-1</sup> and the rotation speeds from 100 to  
 137 3025 rpm. The high onset potential (ca 1.0 V) and half-wave potential (850 mV at the rotation rate of  
 138 1600 rpm) of O<sub>2</sub> reduction at an ultra-low Pt loading ( $1.13 \mu\text{g cm}^{-2}$ ) indicate a good ORR activity of a  
 139 Pt<sub>ML</sub>PdNiN/C catalyst. The kinetic current density ( $j_k$ ) was calculated from these ORR polarization  
 140 curves (Fig. 4a) using the Koutecky-Levich equation [22]:

$$141 \quad \frac{1}{j} = \frac{1}{j_k} + \frac{1}{B\omega} \quad (2)$$

142 where  $j$  is the measured current density,  $B$  and  $\omega$  are the constant and rotation rate, respectively.  
 143 As can be seen from the Koutecky-Levich plot ( $1/j$  plotted as a function of  $\omega^{-1/2}$ ), shown in Fig. 4b,  
 144 the linearity and parallelism of the plots at 0.8 V, 0.85 V and 0.9 V indicate the first-order kinetics with  
 145 respect to molecular oxygen [28]. The intercept with the y-axis gives the inverse kinetic current density.

146 The specific activity was determined from the normalization of kinetic current density to the ECSA  
 147 while the kinetic current density was normalized to the loading of Pt or platinum group metal (PGM) to  
 148 calculate the mass activity. The specific activity of the Pt<sub>ML</sub>PdNiN/C catalyst is 1.17 mA cm<sup>-2</sup> at 0.9 V,  
 149 which is more than 4 times higher than that of commercial Pt/C catalyst (0.24 mA cm<sup>-2</sup>), and 2.5 times  
 150 higher than that of the commercial Pd/C with Pt monolayer (0.42 mA cm<sup>-2</sup>). However, higher ORR  
 151 activities for commercial Pt/C catalyst were observed in some literature [29,30]. The Pt mass activity of  
 152 Pt<sub>ML</sub>PdNiN/C catalyst (1.05 A mg<sup>-1</sup>) is more than 5 times higher than the commercial Pt/C catalyst (0.2  
 153 A mg<sup>-1</sup>) and is also greater than the Pt<sub>ML</sub>Pd/C catalyst (0.95 A mg<sup>-1</sup>) [21].



154

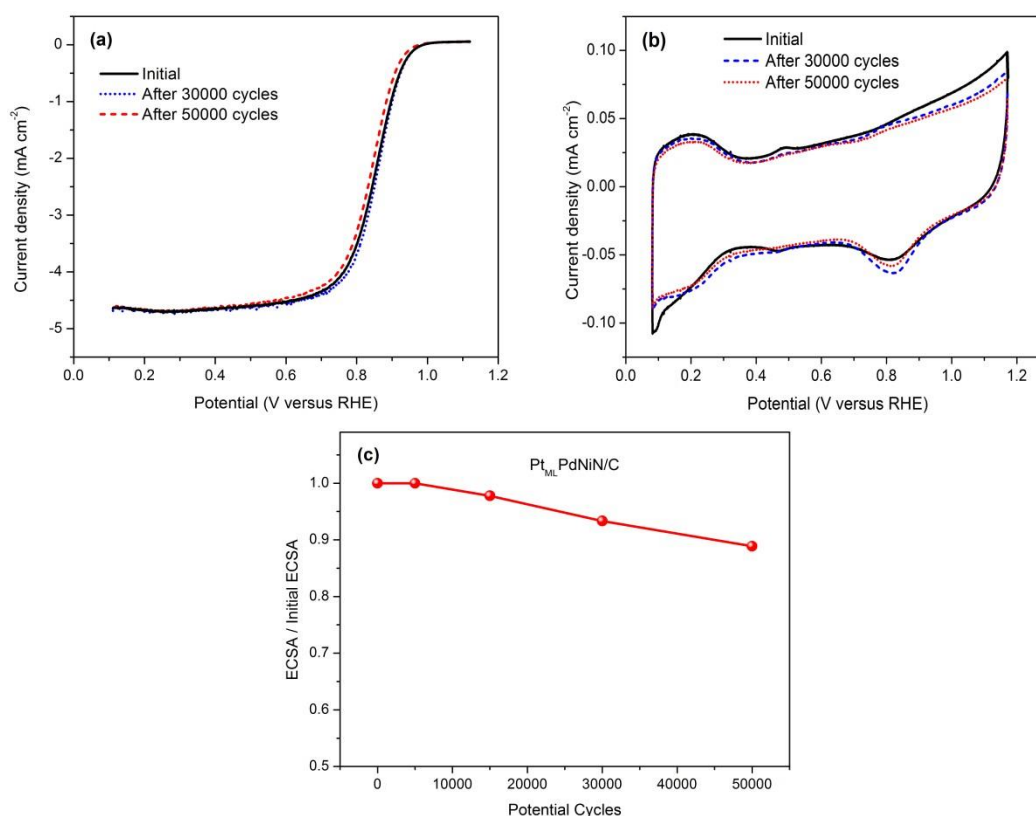
155

156 **Fig. 4.** ORR polarization curves for the Pt<sub>ML</sub>PdNiN/C nanoparticles in 0.1 M HClO<sub>4</sub> solution  
 157 at a scan rate of 10 mV s<sup>-1</sup> at various rpm. (b) The Koutechy-Levich plots at 0.8 V, 0.85 V  
 158 and 0.9 V obtained from the ORR polarization curves as shown in (a). (c) Specific and mass  
 159 activities for the commercial Pt/C, Pt<sub>ML</sub>Pd/C and Pt<sub>ML</sub>PdNiN/C catalysts at 0.9 V.

160 In addition to the high electrochemical activities, the Pt<sub>ML</sub>PdNiN/C catalyst also exhibited excellent  
 161 stability. The stability of the electrocatalyst was evaluated by an accelerated durability test involving  
 162 potential cycling between 0.6 V and 1.0 V at the sweep rate of 50 mV s<sup>-1</sup> using a RDE in an air-saturated  
 163 0.1 M HClO<sub>4</sub> solution at room temperature. Fig. 5a shows the ORR polarization curves of the  
 164 Pt<sub>ML</sub>PdNiN/C catalyst at 1600 rpm before and after 30000 and 50000 potential cycles. After 30000  
 165 cycles, the half-wave potential of the ORR polarization curve remained at almost the initial value. After  
 166 50000 cycles, the ORR measurements showed only 10 mV loss in the half-wave potential. This  
 167 observation is similar to the previous results of Pt<sub>ML</sub>Pd/C nanoparticles that retained their ORR activity  
 168 even after losing their electrochemical surface area (ECSA) [31]. This can be explained by the concept  
 169 that the Pd dissolution in the catalyst induces contraction to the Pt bonds and thereby increases the ORR

170 activity [12,32]. Such a mechanism may be operative in the present system. However, as shown below,  
 171 the loss in ECSA of Pt<sub>ML</sub>PdNiN/C is much smaller than that of Pt<sub>ML</sub>Pd/C, presumably because the  
 172 presence of nitride phase retards the dissolution rate.

173 Fig. 5b shows the CV curves of the Pt<sub>ML</sub>PdNiN/C catalyst in 0.1 M HClO<sub>4</sub> solution before and after  
 174 cycling indicating a negligible loss of Pt surface area. The ECSA losses of the Pt<sub>ML</sub>PdNiN/C catalyst  
 175 after different cycles are shown in Fig. 5c. As reported in our previous paper, the Pt<sub>ML</sub>Pd/C catalyst  
 176 exhibited a drastic decrease in ECSA after electrochemical cycling (27% after 5000 cycles and 34% after  
 177 15000 cycles) due to the dissolution of Pd from the core [21]. Incorporation of Ni in the Pd core can slow  
 178 down the Pd dissolution and as a result decrease the ECSA loss to 11.5% after 5000 cycles. But further  
 179 cycling of the PdNi core leads to an ECSA loss of 28% after 15000 cycles. Nitriding the PdNi core  
 180 restrains the dissolution process, the ECSA loss of the Pt<sub>ML</sub>PdNiN/C catalyst, as shown in Fig. 5c, is  
 181 only 11% after 50000 cycles. By further comparing to the commercial Pt/C catalyst which only retains  
 182 55% of its initial ECSA after 30000 cycles, the less ECSA loss of the obtained Pt<sub>ML</sub>PdNiN/C catalyst  
 183 indicates that stabilization the metal core by nitrogen modification exhibits a significant improvement in  
 184 Pt stability [19]. ORR activities of the Pt<sub>ML</sub>PdNiN/C catalyst before and after an accelerated durability  
 185 test are listed in Table 1.



186

187

188 Fig. 5. (a) ORR polarization curves and (b) cyclic voltammograms of the obtained Pt<sub>ML</sub>PdNiN/C  
 189 catalyst before and after 50000 cycles test between 0.6 and 1.0 V in 0.1 M HClO<sub>4</sub> solution. (c) ECSA  
 190 degradation for Pt<sub>ML</sub>PdNiN/C catalyst plotted as a function of the number of after potential cycles  
 191 between 0.6 and 1.0 V.

192 **Table 1.** Catalytic activities of the Pt<sub>ML</sub>PdNiN/C catalyst before and after the accelerated durability  
 193 test.  
 194

	ECSA (m <sup>2</sup> g <sup>-1</sup> Pt)	E <sub>1/2</sub> (mV)	Specific Activity (mA cm <sup>-2</sup> )	Pt Mass Activity (A mg <sup>-1</sup> )
Initial	90	850	1.17	1.05
After 30000 cycles	84	854	1.35	1.13
After 50000 cycles	80	840	0.84	0.67

### 195 3. Experimental Section

#### 196 3.1. Preparation of PdNiN/C nanoparticles

197 PdNi nanoparticles were synthesized by mixing a 1:1 molar ratio of Pd(NO<sub>3</sub>)<sub>2</sub>·H<sub>2</sub>O and  
 198 Ni(HCO<sub>2</sub>)<sub>2</sub>·2H<sub>2</sub>O salts with high area Vulcan XC-72R carbon black in MilliQ UV-plus water (Millipore,  
 199 18 MΩ) to obtain a total metal loading of 20 wt%. After sonicating the mixture for an hour under  
 200 continuous Ar flow, NaBH<sub>4</sub> was added into the mixture and was then kept under sonication for 1 h. The  
 201 mixture was filtered and rinsed with Millipore water, and then dried. The obtained PdNi/C nanoparticles  
 202 were annealed in N<sub>2</sub> at 250 °C for 1 h followed by annealing at 510 °C for 2 h using NH<sub>3</sub> as the nitrogen  
 203 precursor to get the PdNiN/C nanoparticles.

#### 204 3.2. Characterization

205 The microstructure of the synthesized PdNiN/C nanoparticles was characterized by Hitachi (HD-  
 206 2700C) aberration-corrected STEM using a 1.4 Å electron probe with probe current ~50 pA and an  
 207 energy resolution of 0.35 eV, at the Center for Functional Nanomaterials (CFN), Brookhaven National  
 208 Laboratory (BNL). Elementary sensitive EELS line scan and mapping were carried out for Pd M-edge  
 209 (2122 eV), Ni L-edge (855 eV) across various single PdNiN/C nanoparticle. The XAS measurements  
 210 were undertaken at the National Synchrotron Light Source, BNL using Beam Line X19A. The content of  
 211 Pd and Ni in the PdNiN/C, measured by inductively coupled plasma-optical emission spectrometry  
 212 (ICP-OES), were 8.2 wt% and 7.0 wt% respectively.

#### 213 3.3. Electrochemical measurements

214 Electrochemical testing was carried out in a three-electrode test cell by using a potentiostat (CHI  
 215 700B, CH Instruments). Before testing, catalyst ink was prepared by ultrasonic mixing of 5 mg of  
 216 catalyst with 5 ml Millipore water until a dark and uniform aqueous dispersion was achieved. A thin film  
 217 of the catalyst was prepared on a glassy carbon RDE with the area of 0.196 cm<sup>2</sup> by placing 10-15 μl of  
 218 the obtained dispersion and then covered by a 10μl dilute Nafion solution (2μg μl<sup>-1</sup>). We deposited Pt  
 219 monolayer both on the prepared PdNiN/C nanoparticle and commercial Pd/C nanoparticle surfaces  
 220 using the galvanic displacement of Cu monolayer formed by Cu under-potential deposition (UPD)  
 221 [6,16]. The Pt loadings on the RDE for the Pt<sub>M</sub>L PdNiN/C and Pt<sub>M</sub>L Pd/C catalysts were 1.13 and 3.75 μg  
 222 cm<sup>-2</sup> respectively whereas their Pd loadings were 0.82 and 2.0 μg cm<sup>-2</sup> respectively. However a much  
 223 higher catalyst loading would be required for MEA preparation to replicate the ORR activity as that of  
 224 RDE. The Pt loading on RDE for the commercial Pt/C catalyst was 7.65 μg cm<sup>-2</sup>. The electrochemical

225 measurements were all performed at room temperature, and the potential were referenced to that of the  
226 reversible hydrogen electrode (RHE).

#### 227 4. Conclusions

228 We described a promising route to develop nitride-stabilized substrates for Pt monolayer catalyst with  
229 substantial reduction in platinum group metal loading while retaining high ORR activity and stability.  
230 Using STEM-EELS mapping techniques we have investigated the core-shell structure of the catalyst  
231 while XAS measurement emphasized the NiN<sub>x</sub> species in the core of the nanoparticles providing a stable  
232 support for Pt monolayer electrocatalysts.

#### 233 Acknowledgements

234 This research was performed at Brookhaven National Laboratory under contract DE-SC00112704  
235 with the US Department of Energy, Office of Basic Energy Science, Material Science and Engineering  
236 Division, Division of Chemical Sciences, Geosciences and Biosciences Division. Beam lines X19A at  
237 the NSLS are supported in part by the Synchrotron Catalysis Consortium, U. S. Department of Energy  
238 Grant No DE-FG02-05ER15688. This work was also conducted under the framework of KIER's (Korea  
239 Institute of Energy Research) Research and Development Program (B5-2425).

#### 240 References

- 241 1. Borup, R.; Meyers, J.; Pivovar, B.; Kim, Y.S.; Mukundan, R.; Garland, N.; Myers, D.; Wilson,  
242 M.; Garzon, F.; Wood, D., *et al.* Scientific aspects of polymer electrolyte fuel cell durability  
243 and degradation. *Chem. Rev.* **2007**, *107*, 3904-3951.
- 244 2. Jacobson, M.Z.; Colella, W.G.; Golden, D.M. Cleaning the air and improving health with  
245 hydrogen fuel-cell vehicles. *Science* **2005**, *308*, 1901-1905.
- 246 3. Gasteiger, H.A.; Markovic, N.M. Just a dream-or future reality? *Science* **2009**, *324*, 48-49.
- 247 4. Debe, M.K. Electrocatalyst approaches and challenges for automotive fuel cells. *Nature* **2012**,  
248 *486*, 43-51.
- 249 5. Yasuda, K.; Taniguchi, A.; Akita, T.; Ioroi, T.; Siroma, Z. Platinum dissolution and deposition in  
250 the polymer electrolyte membrane of a pem fuel cell as studied by potential cycling. *Phys.*  
251 *Chem. Chem. Phys.* **2006**, *8*, 746-752.
- 252 6. Adzic, R.; Zhang, J.; Sasaki, K.; Vukmirovic, M.; Shao, M.; Wang, J.; Nilekar, A.; Mavrikakis,  
253 M.; Valerio, J.; Uribe, F. Platinum monolayer fuel cell electrocatalysts. *Top. Catal.* **2007**, *46*,  
254 249-262.
- 255 7. Shao, M.; Shoemaker, K.; Peles, A.; Kaneko, K.; Protsailo, L. Pt monolayer on porous pd-cu  
256 alloys as oxygen reduction electrocatalysts. *J. Am. Chem. Soc.* **2010**, *132*, 9253-9255.
- 257 8. Strasser, P.; Koh, S.; Anniyev, T.; Greeley, J.; More, K.; Yu, C.F.; Liu, Z.C.; Kaya, S.; Nordlund,  
258 D.; Ogasawara, H., *et al.* Lattice-strain control of the activity in dealloyed core-shell fuel cell  
259 catalysts. *Nat Chem* **2010**, *2*, 454-460.
- 260 9. Wang, D.L.; Xin, H.L.L.; Hovden, R.; Wang, H.S.; Yu, Y.C.; Muller, D.A.; DiSalvo, F.J.;  
261 Abruna, H.D. Structurally ordered intermetallic platinum-cobalt core-shell nanoparticles with  
262 enhanced activity and stability as oxygen reduction electrocatalysts. *Nat Mater* **2013**, *12*, 81-  
263 87.
- 264 10. Brimaud, S.; Behm, R.J. Electrodeposition of a pt monolayer film: Using kinetic limitations for

- 265 atomic layer epitaxy. *J Am Chem Soc* **2013**, *135*, 11716-11719.
- 266 11. Zhao, X.; Chen, S.; Fang, Z.; Ding, J.; Sang, W.; Wang, Y.; Zhao, J.; Peng, Z.; Zeng, J.  
267 Octahedral pd@pt<sub>1.8</sub>ni core-shell nanocrystals with ultrathin pt<sub>1</sub> alloy shells as active  
268 catalysts for oxygen reduction reaction. *J. Am. Chem. Soc.* **2015**, *137*, 2804-2807.
- 269 12. Wang, J.X.; Inada, H.; Wu, L.J.; Zhu, Y.M.; Choi, Y.M.; Liu, P.; Zhou, W.P.; Adzic, R.R.  
270 Oxygen reduction on well-defined core-shell nanocatalysts: Particle size, facet, and pt shell  
271 thickness effects. *J. Am. Chem. Soc.* **2009**, *131*, 17298-17302.
- 272 13. Karan, H.I.; Sasaki, K.; Kuttiyiel, K.; Farberow, C.A.; Mavrikakis, M.; Adzic, R.R. Catalytic  
273 activity of platinum mono layer on iridium and rhenium alloy nanoparticles for the oxygen  
274 reduction reaction. *Acs Catal* **2012**, *2*, 817-824.
- 275 14. Zhang, Y.; Hsieh, Y.C.; Volkov, V.; Su, D.; An, W.; Si, R.; Zhu, Y.M.; Liu, P.; Wang, J.X.; Adzic,  
276 R.R. High performance pt mono layer catalysts produced via core-catalyzed coating in ethanol.  
277 *Acs Catal.* **2014**, *4*, 738-742.
- 278 15. Zhang, Y.; Ma, C.; Zhu, Y.M.; Si, R.; Cai, Y.; Wang, J.X.; Adzic, R.R. Hollow core supported pt  
279 monolayer catalysts for oxygen reduction. *Catal. Today* **2013**, *202*, 50-54.
- 280 16. Kuttiyiel, K.A.; Sasaki, K.; Choi, Y.; Su, D.; Liu, P.; Adzic, R.R. Bimetallic ir<sub>1</sub>ni core platinum  
281 monolayer shell electrocatalysts for the oxygen reduction reaction. *Energy Environ. Sci.* **2012**,  
282 *5*, 5297-5304.
- 283 17. Hsieh, Y.-C.; Zhang, Y.; Su, D.; Volkov, V.; Si, R.; Wu, L.; Zhu, Y.; An, W.; Liu, P.; He, P., *et al.*  
284 Ordered bilayer ruthenium-platinum core-shell nanoparticles as carbon monoxide-tolerant fuel  
285 cell catalysts. *Nat. Commun.* **2013**, *4*, 1-9.
- 286 18. Zhang, J.; Vukmirovic, M.B.; Xu, Y.; Mavrikakis, M.; Adzic, R.R. Controlling the catalytic  
287 activity of platinum-monolayer electrocatalysts for oxygen reduction with different substrates.  
288 *Angew. Chem. Int. Ed.* **2005**, *44*, 2132-2135.
- 289 19. Zhang, J.; Sasaki, K.; Sutter, E.; Adzic, R.R. Stabilization of platinum oxygen-reduction  
290 electrocatalysts using gold clusters. *Science* **2007**, *315*, 220-222.
- 291 20. Gong, K.; Su, D.; Adzic, R.R. Platinum-monolayer shell on auni<sub>0.5</sub>fe nanoparticle core  
292 electrocatalyst with high activity and stability for the oxygen reduction reaction. *J. Am. Chem.*  
293 *Soc.* **2010**, *132*, 14364-14366.
- 294 21. Kuttiyiel, K.A.; Sasaki, K.; Su, D.; Vukmirovic, M.B.; Marinkovic, N.S.; Adzic, R.R. Pt  
295 monolayer on au-stabilized pd<sub>1</sub>ni core-shell nanoparticles for oxygen reduction reaction.  
296 *Electrochim. Acta* **2013**, *110*, 267-272.
- 297 22. Kuttiyiel, K.A.; Sasaki, K.; Choi, Y.M.; Su, D.; Liu, P.; Adzic, R.R. Nitride stabilized pt<sub>1</sub>ni  
298 core-shell nanocatalyst for high oxygen reduction activity. *Nano Lett.* **2012**, *12*, 6266-6271.
- 299 23. Kuttiyiel, K.A.; Choi, Y.; Hwang, S.-M.; Park, G.-G.; Yang, T.-H.; Su, D.; Sasaki, K.; Liu, P.;  
300 Adzic, R.R. Enhancement of the oxygen reduction on nitride stabilized pt-m (m=fe, co, and ni)  
301 core-shell nanoparticle electrocatalysts. *Nano Energy* **2015**, *13*, 442-449.
- 302 24. Liu, H.; Koenigsmann, C.; Adzic, R.R.; Wong, S.S. Probing ultrathin one-dimensional pd-ni  
303 nanostructures as oxygen reduction reaction catalysts. *ACS Catal.* **2014**, *4*, 2544-2555.
- 304 25. Subbaraman, R.; Tripkovic, D.; Strmcnik, D.; Chang, K.-C.; Uchimura, M.; Paulikas, A.P.;  
305 Stamenkovic, V.; Markovic, N.M. Enhancing hydrogen evolution activity in water splitting by  
306 tailoring li<sup>+</sup>-ni(o<sub>h</sub>)<sub>2</sub>-pt interfaces. *Science* **2011**, *334*, 1256-1260.
- 307 26. Chu, Y.-Y.; Wang, Z.-B.; Gu, D.-M.; Yin, G.-P. Performance of pt/c catalysts prepared by  
308 microwave-assisted polyol process for methanol electrooxidation. *J. Power Sources* **2010**, *195*,  
309 1799-1804.
- 310 27. Schmidt, T.J.; Gasteiger, H.A.; Stäb, G.D.; Urban, P.M.; Kolb, D.M.; Behm, R.J.

- 311 Characterization of high - surface - area electrocatalysts using a rotating disk electrode  
312 configuration. *J. Electrochem. Soc.* **1998**, *145*, 2354-2358.
- 313 28. Sasaki, K.; Wang, J.X.; Naohara, H.; Marinkovic, N.; More, K.; Inada, H.; Adzic, R.R. Recent  
314 advances in platinum monolayer electrocatalysts for oxygen reduction reaction: Scale-up  
315 synthesis, structure and activity of pt shells on pd cores. *Electrochim. Acta* **2010**, *55*, 2645-  
316 2652.
- 317 29. Garsany, Y.; Singer, I.L.; Swider-Lyons, K.E. Impact of film drying procedures on rde  
318 characterization of pt/vc electrocatalysts. *J Electroanal Chem* **2011**, *662*, 396-406.
- 319 30. Takahashi, I.; Kocha, S.S. Examination of the activity and durability of pemfc catalysts in  
320 liquid electrolytes. *J Power Sources* **2010**, *195*, 6312-6322.
- 321 31. Sasaki, K.; Naohara, H.; Cai, Y.; Choi, Y.M.; Liu, P.; Vukmirovic, M.B.; Wang, J.X.; Adzic,  
322 R.R. Core-protected platinum monolayer shell high-stability electrocatalysts for fuel-cell  
323 cathodes. *Angew. Chem. Int. Ed.* **2010**, *49*, 8602-8607.
- 324 32. Wang, J.X.; Ma, C.; Choi, Y.M.; Su, D.; Zhu, Y.M.; Liu, P.; Si, R.; Vukmirovic, M.B.; Zhang,  
325 Y.; Adzic, R.R. Kirkendall effect and lattice contraction in nanocatalysts: A new strategy to  
326 enhance sustainable activity. *J. Am. Chem. Soc.* **2011**, *133*, 13551-13557.

327 © 2015 by the authors; licensee MDPI, Basel, Switzerland. This article is an open access article  
328 distributed under the terms and conditions of the Creative Commons Attribution license  
329 (<http://creativecommons.org/licenses/by/4.0/>).

## Supplementary Information

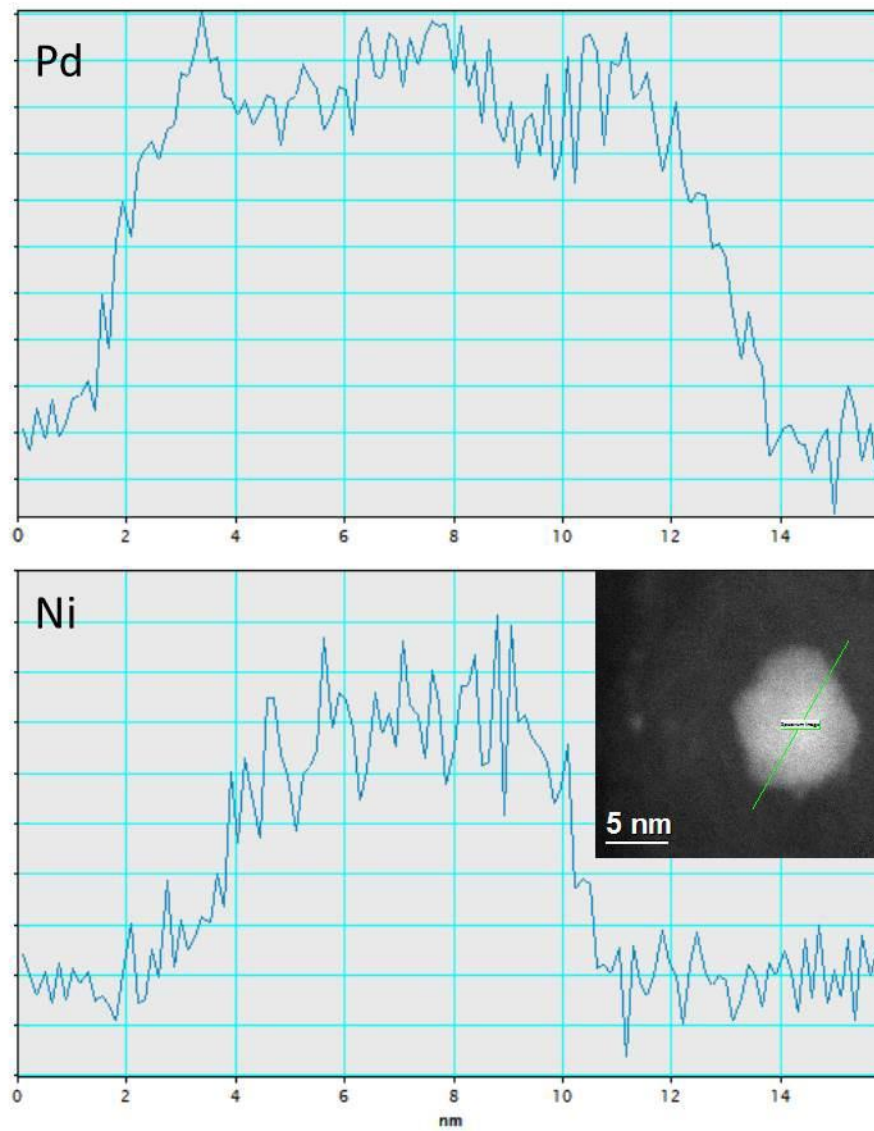


**Fig.S1.** EELS line scan profile for Pd M-edge and Ni L-edge from a single nanoparticle along the scanned line as indicated in the inset.

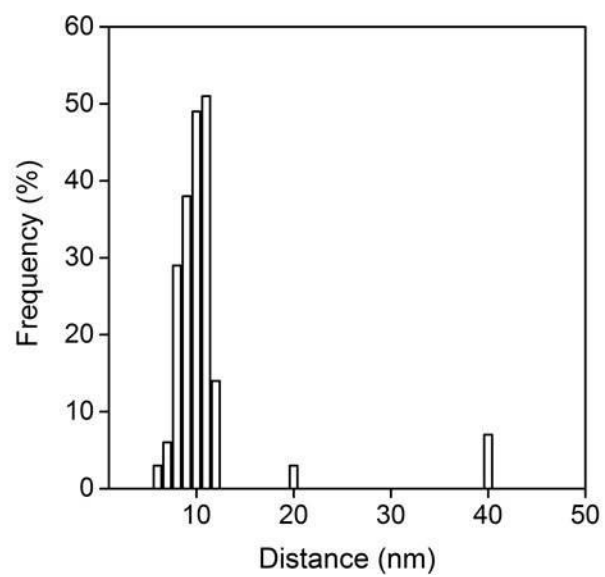
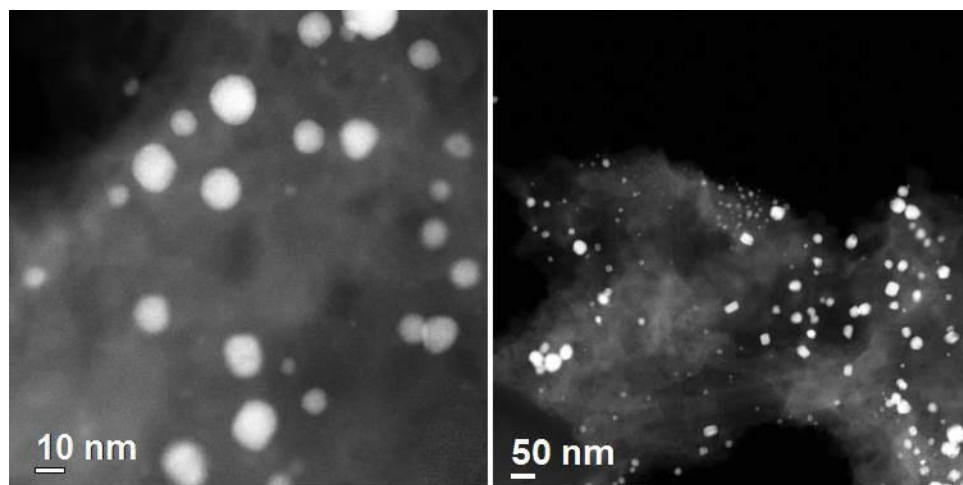


**Fig.S2.** HAADF-STEM images of the PdNiN/C catalyst along with particle size distribution of the nanoparticles (sample size=200).